On the data dependent filtration techniques in the single-photon emission computed tomography

Jean-Pol Guillement, Roman Novikov

On the data dependent filtration techniques in the single-photon emission computed tomography

J.-P.Guillement and R.G.Novikov

CNRS, Laboratoire de Mathématiques Jean Leray (UMR 6629), Université de Nantes, BP 92208, F-44322, Nantes cedex 03, France

E-mail: guillement@math.univ-nantes.fr and novikov@math.univ-nantes.fr

Abstract

We develop space variant data dependent filtration techniques for single-photon emission computed tomography (SPECT) data modeled as the 2D attenuated ray transform with Poisson noise. In these studies we proceed, in particular, from some results of our recent work [J.-P.Guillement, R.G.Novikov, A noise property analysis of single-photon emission computed tomography data, Inverse Problems 20, pp.175-198, (2004)]. We illustrate our filtrations in the framework of simulated SPECT imaging involving (generalized and classical) FBP algorithms.

1. Introduction

In the single-photon emission computed tomography (SPECT) one considers a body containing radioactive isotopes emitting photons. The emission data in SPECT consists in the radiation measured outside the body by a family of detectors during some fixed time. The basic problem of SPECT consists in finding the distribution of the radioactive isotopes in the body from the emission data and some a priori information concerning the body. Usually this a priori information consists in the photon attenuation coefficient in the points of body, where this coefficient is found in advance by the methods of the transmission computed tomography (under some conditions, this coefficient can be also approximately found directly from the emission data in the frameworks of the "identification" problem). In 2D SPECT, that is when the problem is restricted to a fixed two-dimensional plane Ξ intersecting the body and identified with $\mathbb{R}^2$, the emission data are modeled, in some approximation, as a function p on the detector set Γ (see formulas (1.3), (1.4) given below) or by other words as the 2D attenuated ray transform with Poisson noise. Let us remind now related mathematical definitions.

The 2D attenuated ray transformation P_a is defined by the formula

$$\begin{aligned} &P_a f(\gamma) = \int\limits_{\mathbb{R}} \exp\left(-\mathcal{D}a(s\theta^\perp + t\theta, \theta)\right) f(s\theta^\perp + t\theta)dt, \\ &\gamma = (s,\theta) \in \mathbb{R}\times\mathbb{S}^1, \quad \theta^\perp = (-\theta_2, \theta_1) \quad \text{for} \quad \theta = (\theta_1,\theta_2) \in \mathbb{S}^1, \end{aligned} \tag{1.1a}$$

$$\mathcal{D}a(x,\theta) = \int\limits_0^{+\infty} a(x+t\theta)dt, \quad (x,\theta) \in \mathbb{R}^2\times\mathbb{S}^1, \tag{1.1b}$$

where a and f are real-valued, sufficiently regular functions on $\mathbb{R}^2$ with sufficient decay at infinity, a is a parameter (the attenuation coefficient), $\mathcal{D}a$ is the divergent beam transform

of a, f is a test function. In (1.1a) we interpret $\mathbb{R}\times\mathbb{S}^1$ as the set of all oriented straight lines in $\mathbb{R}^2$. If $\gamma=(s,\theta)\in\mathbb{R}\times\mathbb{S}^1$, then $\gamma=\{x\in\mathbb{R}^2:\ x=s\theta^\perp+t\theta,\ t\in\mathbb{R}\}$ (modulo orientation) and θ gives the orientation of γ.

In SPECT, $f\geq 0$ is the density of radioactive isotopes, $a\geq 0$ is the linear photon attenuation coefficient of the medium, and (in some approximation) CP_af is the expected emission data (the expected sinogram), where C is a positive constant depending on detection parameters.

More precisely, saying about the emission data in 2D SPECT, we assume that

$$a(x)\geq 0,\ f(x)\geq 0,\quad \text{for}\ \ x\in\mathbb{R}^2,\ a(x)\equiv 0,\quad f(x)\equiv 0\ \ \text{for}\ \ |x|\geq R \tag{1.2}$$

and consider in $\mathbb{R}\times\mathbb{S}^1$ a discrete subset of the form

$$\begin{aligned}&\Gamma=\{\gamma_{i,j}=(s_i,\theta(\varphi_j)):\ s_i=-R+(i-1)\Delta s,\ \varphi_j=(j-1)\Delta\varphi,\\ &\Delta s=2R/(n_s-1),\ \Delta\varphi=2\pi/n_\varphi,\quad i=1,\dots,n_s,\ j=1,\dots,n_\varphi\},\end{aligned} \tag{1.3}$$

where $\theta(\varphi)=(\cos\varphi,\sin\varphi)$, R is the radius of image support of ((1.2), n_s, n_φ are sufficiently large natural numbers, and n_φ is even. We say that Γ is a detector set.

In 2D SPECT, in some approximation, the emission data consist of a function p on Γ, where

$$\begin{aligned}&p(\gamma)\ \ \text{is a realization of a Poisson variate}\ \ \mathbf{p}(\gamma)\\ &\text{with the mean}\ \ M\mathbf{p}(\gamma)=g(\gamma)=CP_af(\gamma)\ \ \text{for any}\ \ \gamma\in\Gamma\\ &\text{and all}\ \ \mathbf{p}(\gamma),\ \ \gamma\in\Gamma,\ \ \text{are independent.}\end{aligned} \tag{1.4}$$

In addition, it is assumed that $C=C_1t$, where t is the detection time per projection and C_1 is independent of t. We say that p of (1.4) is the 2D attenuated ray transform (CP_af on Γ) with Poisson noise.

For more information concerning the aforementioned basic points of SPECT, see, for example, [NW], [LM], [Br] and references therein.

In the present work we consider the following two problems:

Problem 1. Find (as well as possible) $g=CP_af$ on Γ from the emission data p on Γ (of (1.4), (1.3)).

Problem 2. Find (as well as possible) the distribution Cf on $\mathbb{R}^2$ from the emission data p on Γ (of (1.4), (1.3)) and (approximately known) attenuation coefficient a on $\mathbb{R}^2$.

(Note that in Problems 1 and 2 we assume that a, f satisfy (1.2) and are sufficiently regular real-valued functions on $\mathbb{R}^2$, $C>0$.)

In the present work we develop, first, the data dependent filtration techniques for solving Problem 1, see Section 2. As a result, we propose, in particular, a filtration (consisting, in general, of two steps) of the form

$$p\overset{W_1}{\to}\ \tilde p\overset{W_2}{\to}\ \tilde{\tilde p}, \tag{1.5}$$

$$\tilde p(\gamma)=\sum_{\gamma'\in\mathcal{D}_{\gamma,l,m}}W_1(\gamma,\gamma',p,\varepsilon_1,l,m)p(\gamma'),\quad \gamma\in\Gamma, \tag{1.6}$$

$$\tilde{\tilde p}(\gamma)=\sum_{\gamma'\in\Gamma}W_2(\gamma,\gamma',p,\tilde p,\alpha,\varepsilon_2)\tilde p(\gamma'),\quad \gamma\in\Gamma, \tag{1.7}$$

where $W_1(\gamma, \gamma', p, \varepsilon_1, l, m)$ at fixed γ depends only on local characteristics of p on a neighborhood $\mathcal{D}_{\gamma,l,m}$ of γ in Γ of a sufficiently small size $l \times m$, in particular, it depends on the noise level of p on $\mathcal{D}_{\gamma,l,m}$, $W_2(\gamma, \gamma', p, \tilde{p}, \beta)$ depends on global spectral characteristics of p and $\tilde{p}$, and ε_1, α, ε_2 are filter parameters. (Note that W_1 is space variant and W_2 is space invariant in the present work.) In these studies we proceed from the work [GN] as regards W_1 of (1.5), (1.6) and from the works [RL], [GB], [GouNol], [GN] as regards W_2 of (1.5)-(1.7).

Second, we apply our results on Problem 1 for solving Problem 2 by means of techniques for finding Cf from CP_af and a for the noiseless case (or more precisely for the case when the transform CP_af given on Γ is free from an intensive random noise). In the framework of these techniques we use, in particular, the explicit inversion formula of [No] and the iterative inversion method of [MNOY]. Related results are reminded in Section 3.

In addition, in connection with Problems 1 and 2 we observed that if a is strongly nonuniform in a neighborhood of a region where f is of particular interest (see phantom 2 of Section 4), then to reconstruct Cf properly, it may be important to smooth a in a consistent way with filtering p. More precisely, if p is filtered as

$$p \to Wp, \quad \text{where} \quad Wp(\gamma) = \sum_{\gamma' \in \Gamma} W(\gamma, \gamma', p)p(\gamma'), \quad \gamma \in \Gamma, \tag{1.8}$$

then it may be important to smooth a as

$$a \to P_0^{-1}WP_0a, \quad \text{where} \quad WP_0a(\gamma) = \sum_{\gamma' \in \Gamma} W(\gamma, \gamma', p)P_0a(\gamma'), \quad \gamma \in \Gamma, \tag{1.9}$$

where P_0 denotes the classical (non-attenuated) ray transformation.

Numerical examples illustrating possibilities of our filtrations (1.5)-(1.7) are given in Section 4.

2. Two-step data dependent filtration W_2W_1

2.1. *Space variant filtration W_1 of the first step.* In this subsection we construct our space variant filtration W_1 of (1.5), (1.6). Let

$$\begin{aligned} &\mathcal{D}_{\gamma,l,m} = \{\gamma' = (s', \theta(\varphi')) \in \Gamma : \ -[(l-1)/2]\Delta s \le s' - s \le [l/2]\Delta s, \\ &-[(m-1)/2]\Delta\varphi \le \varphi' - \varphi \le [m/2]\Delta\varphi\} \\ &\text{for} \quad \gamma = (s, \theta(\varphi)) \in \Gamma \quad \text{and} \quad l, m \in \mathbb{N}, \end{aligned} \tag{2.1}$$

where $[\lambda]$ is the integer part of real positive λ, $\theta(\varphi)$, Δs, $\Delta\varphi$ are the same that in (1.3), $\varphi' \in \mathbb{R}$. One can see that $\mathcal{D}_{\gamma,l,m}$ is a neighborhood of γ in Γ. If $\gamma = (s, \theta(\varphi)) \in \Gamma$,

$$-R \le s - [(l-1)/2]\Delta s, \quad s + [l/2]\Delta s \le R \tag{2.2}$$

and $m < n_\varphi$ (where n_φ is the number of (1.3)), then $\mathcal{D}_{\gamma,l,m}$ contains $l \times m$ points of Γ.

Let

$$\|q\|_{L^\alpha(\mathcal{D})} = (\Delta s \Delta\varphi \sum_{\gamma \in \mathcal{D}} |q(\gamma)|^\alpha)^{1/\alpha}, \tag{2.3}$$

where q is a test functions on $\mathcal{D} \subseteq \Gamma$, $\alpha \in \mathbb{N}$. Let

$$\zeta(q_2, q_1, \mathcal{D}) = \frac{\|q_2 - q_1\|_{L^2(\mathcal{D})}}{\|q_1\|_{L^2(\mathcal{D})}}, \tag{2.4}$$

where q_1, q_2 are test functions on $\mathcal{D} \subseteq \Gamma$. For p and g of (1.4) and $\mathcal{D} \subseteq \Gamma$ the quantity $\zeta(p, g, \mathcal{D})$ is the noise level (in the L^2-sense) of p on $\mathcal{D}$. Under the condition that l and m are not too small, following [GN], we use the formula

$$\zeta(p, g, \mathcal{D}_{\gamma,l,m}) \approx \left(\frac{\|p\|_{L^1(\mathcal{D}_{\gamma,l,m})}}{\|p\|^2_{L^2(\mathcal{D}_{\gamma,l,m})} - \|p\|_{L^1(\mathcal{D}_{\gamma,l,m})}} \right)^{1/2}, \quad \gamma \in \Gamma. \tag{2.5}$$

Under the condition that $l \ll n_s$, $m \ll n_\varphi$ (where n_s, n_φ are the numbers of (1.3)), the noise level $\zeta(p, g, \mathcal{D}_{\gamma,l,m})$ may differ considerably for different $\gamma \in \Gamma$. In particular, because of this reason, one has to use, in general, a space variant filtration for p in order to solve properly Problem 1. To construct our space variant data dependent filtration W_1 of (1.5), (1.6) we proceed from space invariant data dependent filtrations (based on results of [GN]) on $\mathcal{D}_{\gamma,l,m}$, $\gamma \in \Gamma$.

Note that if $\gamma = (s, \theta(\varphi)) \in \Gamma$ and $l \in \mathbb{N}$ satisfy (2.2) and $m < n_\varphi$, then $\mathcal{D}_{\gamma,l,m}$ can be identified with

$$I_{l,m} = \{(i_1, i_2) \in \mathbb{Z}^2 : \ 0 \le i_1 \le l-1, \ \ 0 \le i_2 \le m-1\}. \tag{2.6}$$

Let, for example, l and m be even and

$$\hat{I}_{l,m} = \{(j_1, j_2) \in \mathbb{Z}^2 : \ -\frac{l}{2} \le j_1 \le \frac{l}{2} - 1, \ \ -\frac{m}{2} \le j_2 \le \frac{m}{2} - 1\}. \tag{2.7}$$

Let $F_{l,m}$ denote the 2D discrete Fourier transformation defined by

$$\begin{aligned} (F_{l,m}q)(j_1, j_2) = \frac{1}{\sqrt{lm}} \sum_{(i_1,i_2)\in I_{l,m}} q(i_1, i_2) \times \\ \exp\left(-2\pi i \left(\frac{j_1 i_1}{l} + \frac{j_2 i_2}{m}\right)\right), \quad (j_1, j_2) \in \hat{I}_{l,m}, \quad i = \sqrt{-1}, \end{aligned} \tag{2.8}$$

where q is a test function on $I_{l,m}$. Let

$$W_{l,m}(\omega)q = F^{-1}_{l,m} \hat{W}_{l,m}(\omega) F_{l,m} q, \tag{2.9}$$

where

$$\big(\hat{W}_{l,m}(\omega)F_{l,m}q\big)(j_1, j_2) = \hat{W}_{l,m}(j_1, j_2, \omega)(F_{l,m}q)(j_1, j_2), \tag{2.10}$$

$$\begin{aligned} &\hat{W}_{l,m}(j_1, j_2, \omega) = \left(sinc\left(\frac{2\pi j_1}{\omega l}\right) sinc\left(\frac{2\pi j_2}{\omega m}\right)\right)^2 \\ &\text{for} \ \ |j_1| \le \omega\frac{l}{2}, \ \ |j_2| \le \omega\frac{m}{2}, \\ &\hat{W}(j_1, j_2, \omega) = 0 \ \ \text{for} \ \ |j_1| > \omega\frac{l}{2} \ \ \text{or} \ \ |j_2| > \omega\frac{m}{2}, \end{aligned} \tag{2.11}$$

where $sinc(z) = z^{-1}\sin(z)$, q is a test function on $I_{l,m}$, $(j_1, j_2) \in \hat{I}_{l,m}$, ω is a positive real number. Note that $W_{l,m}(\omega)$ is a space invariant data independent filter (dependent on the parameter ω) on $I_{l,m}$ (considered as a discrete torus).

Assuming that $\gamma \in \Gamma$ and $m < n_\varphi$, we consider the identification operators

$$\Lambda_{\gamma,l,m} : \ L^2(\mathcal{D}_{\gamma,l,m}) \to L^2(I_{l,m}), \tag{2.12}$$

$$\begin{aligned} &\big(\Lambda_{\gamma,l,m}p\big)(i_1,i_2) = p(\gamma'(\gamma,i_1,i_2)) \ \text{ for } \ \gamma'(\gamma,i_1,i_2) \in \Gamma, \\ &\big(\Lambda_{\gamma,l,m}p\big)(i_1,i_2) = 0 \ \text{ for } \ \gamma'(\gamma,i_1,i_2) \notin \Gamma, \end{aligned} \tag{2.13}$$

$$\Lambda^*_{\gamma,l,m} : \ L^2(I_{l,m}) \to L^2(\mathcal{D}_{\gamma,l,m}), \tag{2.14}$$

$$(\Lambda^*_{\gamma,l,m}q)(\gamma'(\gamma,i_1,i_2)) = q(i_1,i_2) \ \text{ for } \ \gamma'(\gamma,i_1,i_2) \in \Gamma, \tag{2.15}$$

where

$$\begin{aligned} &\gamma'(\gamma,i_1,i_2) = (s - [(l-1)/2]\Delta s + i_1\Delta s, \theta(\varphi - [(m-1)/2]\Delta\varphi + i_2\Delta\varphi)) \\ &\text{for } \ \gamma = (s,\theta(\varphi)), \end{aligned} \tag{2.16}$$

$(i_1, i_2) \in I_{l,m}$, p is a test function on $\mathcal{D}_{\gamma,l,m}$, q is a test function on $I_{l,m}$. Let

$$W_{\gamma,l,m}(\omega) = \Lambda^*_{\gamma,l,m}W_{l,m}(\omega)\Lambda_{\gamma,l,m}, \quad \gamma \in \Gamma, \quad m < n_\varphi. \tag{2.17}$$

The operator $W_{\gamma,l,m}(\omega)$ is a space invariant (at least near γ which is not too close to the boundary of Γ and for l, m, which are not too small) data independent filter (dependent on the parameter ω) on $\mathcal{D}_{\gamma,l,m}$.

Now we use the principle that for p of (1.4), for $\gamma \in \Gamma$ and under the condition that l and m are not too small or too large, the filtration result $W_{\gamma,l,m}(\omega)\big(p\big|_{\mathcal{D}_{\gamma,l,m}}\big)$ is the most optimal near γ if ω satisfies the equation

$$\zeta\big(p, W_{\gamma,l,m}(\omega)p, \mathcal{D}_{\gamma,l,m}\big) = \varepsilon_1\zeta_{appr,\gamma,l,m}(p), \tag{2.18a}$$

where

$$\zeta_{appr,\gamma,l,m}(p) = \left(\frac{\|p\|_{L^1(\mathcal{D}_{\gamma,l,m})}}{\|p\|^2_{L^2(\mathcal{D}_{\gamma,l,m})} - \|p\|_{L^1(\mathcal{D}_{\gamma,l,m})}}\right)^{1/2}, \tag{2.18b}$$

($\zeta_{appr,\gamma,l,m}(p)$ coincides with the right-hand side of (2.5)), $p = p\big|_{\mathcal{D}_{\gamma,l,m}}$ and ε_1 is slightly smaller or equal to 1. This principle is a local version of the principle proposed in [GN] for global space invariant data dependent filtering on Γ (see Sections 2 and 6 of [GN]). If

$$\mathcal{D}_{\gamma,l,m} = \Gamma, \quad \gamma \in \Gamma, \quad l = n_s, \quad m = n_\varphi, \tag{2.19}$$

then $W_{\gamma,l,m}(\omega)$ of (2.17) with ω of (2.18) is reduced to the space invariant filter $W(\omega)$ with the optimal frequency ω of [GN]. An algorithm for finding ω from (2.18) is, actually, given in Section 6 of [GN] and is based on the bisection method. The only new point

concerning this algorithm is that now when l and m are not very large it is possible that $\zeta\big(p, W_{\gamma,l,m}(\omega)p, \mathcal{D}_{\gamma,l,m}\big)$ remains smaller than $\zeta_{appr,\gamma,l,m}(p)$ even for $\omega \to 0$. In the latter case we take $\omega = \omega_{min}$, where $\omega_{min} > 0$ is fixed in advance. Under the assumption that

$$C_1 l \le m \le C_2 l \quad \text{for some fixed positive} \quad C_1 \quad \text{and} \quad C_2, \tag{2.20}$$

the aforementioned algorithm for finding ω from (2.18) requires $O(l^2 \log l)$ operations; see Section 6 of [GN].

Finally, we define W_1 of (1.5) by the formula

$$(W_1 p)(\gamma) = \big(W_{\gamma,l,m}(\omega)\big(p\big|_{\mathcal{D}_{\gamma,l,m}}\big)\big)(\gamma), \quad \gamma \in \Gamma, \tag{2.21}$$

where $\omega = \omega(\gamma, l, m, p\big|_{\mathcal{D}_{\gamma,l,m}}, \varepsilon_1)$ is found from (2.18). One can see that $\tilde{p} = W_1 p$ defined by (2.21) can be written as (1.6), where ε_1 is the parameter of (2.18). For fixed ε_1, l, m, under the condition (2.20), our filtration $W_1 p$ on Γ requires $n_s n_\varphi O(l^2 \log l)$ operations. If l is sufficiently small, then this quantity of operations is acceptable for numerical implementations.

Note that in our numerical examples we obtained that our space variant data dependent filtration W_1 gives the best results $\tilde{p} = W_1 p$ in the sense of the relative error $\zeta(\tilde{p}, g, \Gamma)$, where ζ is defined by (2.4) and g is the noiseless data of (1.4), if (actually) $\varepsilon_1 = 1$ in (2.18). It is important to note also that in our numerical examples we obtained that

$$\zeta(p, \tilde{p}, \Gamma) \quad \text{is slightly smaller than} \quad \zeta_{appr}(p), \tag{2.22}$$

where $\tilde{p} = W_1 p$ is realized according to (2.17)-(2.19), (2.21), $\varepsilon_1 = 1$, and

$$\zeta_{appr}(p) = \left(\frac{\|p\|_{L^1(\Gamma)}}{\|p\|^2_{L^2(\Gamma)} - \|p\|_{L^1(\Gamma)}} \right)^{1/2}. \tag{2.23}$$

In addition, $\zeta_{appr}(p)$ well coincides with $\zeta(p, g, \Gamma)$ (where g is the noiseless data of (1.4)). The property (2.22) can be explained by the observation that $\Lambda_{\gamma,l,m} p$ on $I_{l,m}$ (considered in $F_{l,m}$ as a discrete torus) is irregular not only because of the Poisson noise in p but also because of discontinuities of $\Lambda_{\gamma,l,m} g$ on $I_{l,m}$ considered as the discrete torus (where g is the function of (1.4)).

2.2. *Space invariant filtration W_2 of the second step.* In this subsection we construct our space invariant filtration W_2 of (1.5), (1.7). Note that Γ can be identified with I_{n_s,n_φ} (where $I_{l,m}$ is defined by (2.6)). Let us suppose that n_φ and n_s of (1.3) are even. Consider $F = F_{n_s,n_\varphi}$ (where $F_{l,m}$ is defined by (2.8)). Consider identification operators

$$\Lambda : \ L^2(\Gamma) \to L^2(I_{n_s,n_\varphi}), \tag{2.24}$$

$$(\Lambda p)(i_1, i_2) = p(\gamma_{i_1,i_2}), \quad (i_1, i_2) \in I_{n_s,n_\varphi}, \tag{2.25}$$

$$\Lambda^* : \ L^2(I_{n_s,n_\varphi}) \to L^2(\Gamma), \tag{2.26}$$

$$(\Lambda^* q)(\gamma_{i_1,i_2}) = q(i_1, i_2), \quad (i_1, i_2) \in I_{n_s,n_\varphi}, \tag{2.27}$$

where $\gamma_{i,j}$ is defined in (1.3), p is a test function on Γ, q is a test function on I_{n_s,n_φ}. Our space invariant filtration W_2 is based, mainly, on the following principles:

(1) The Fourier transform $\hat{g} = F\Lambda g$, where g is the function of (1.4) (that is $g = CP_a f\big|_\Gamma$), is supported mainly in some rather specific domain dependent on f and a; see [RL], [GouNol] and figure 2(b) of the present paper.

(2) The formula holds ([GB]):

$$\begin{aligned} &M|\hat{\mathbf{p}}(j_1,j_2)|^2 = |\hat{g}(j_1,j_2)|^2 + \sum_{\gamma\in\Gamma} g(\gamma), \\ &\hat{\mathbf{p}} = F\Lambda\mathbf{p}, \quad \hat{g} = F\Lambda g, \quad (j_1,j_2)\in \hat{I}_{n_s,n_\varphi}, \end{aligned} \tag{2.28}$$

where $\mathbf{p}$ is the Poisson field of (1.4), g is the function of (1.4), M denotes the mathematical expectation (and $g = M\mathbf{p}$). The formula (2.28) is illustrated also by figure 3(b) of the present paper.

(3) The functions $|\hat{\tilde{p}}|$ and $|\hat{g}|$, where $\hat{\tilde{p}} = F\Lambda\tilde{p}$, $\hat{g} = F\Lambda g$ and $\tilde{p} = W_1 p$ is defined in (1.5), (1.6), (2.21) with $\varepsilon = 1$, g is the function of (1.4), look very similar (especially concerning their support domains); see figures 2(b), 5(b) of the present paper.

From figure 5(b) one can see that $|\hat{\tilde{p}}|$ and, in particular, the set $\mathcal{A} \subset \hat{I}_{n_s,n_\varphi}$, where $|\hat{\tilde{p}}|$ is essentially nonzero, are rather irregular. To present our filtration W_2 of (1.5), (1.7) we construct first

$$\begin{aligned} \rho_\alpha(j_1,j_2) = &\sum_{(j_1',j_2')\in\hat{I}_{n_s,n_\varphi}} G(|j_1-j_1'|,|j_2-j_2'|,\alpha)\times \\ &|\hat{\tilde{p}}|(j_1',j_2'), \quad (j_1,j_2)\in\hat{I}_{n_s,n_\varphi}, \end{aligned} \tag{2.29}$$

where (for example)

$$\begin{aligned} G(j_1,j_2,\alpha) = c(\alpha,n)\exp\left(-\alpha(j_1^2+j_2^2)\right) \quad &\text{for} \quad |j_1|\le n,\ |j_2|\le n, \\ G(j_1,j_2,\alpha) = 0 \quad &\text{for } |j_1|>n \text{ or } |j_2|>n, \\ c(\alpha,n) = \Big(\sum_{|j_1|\le n,|j_2|\le n} &\exp\left(-\alpha(j_1^2+j_2^2)\right)\Big)^{-1}, \quad (j_1,j_2)\in\mathbb{Z}^2, \end{aligned} \tag{2.30}$$

for some parameters $\alpha > 0$ and $n \in \mathbb{N}$.

The function ρ_α is a regularization of $|\hat{\tilde{p}}|$.

We construct W_2 as follows:

$$W_2\tilde{p} = \Lambda^* F^{-1}\hat{W}_2\hat{\tilde{p}}, \quad \hat{\tilde{p}} = F\Lambda\tilde{p}, \tag{2.31}$$

$$W_2\hat{\tilde{p}}(j_1,j_2) = \hat{W}_2(j_1,j_2,\rho_\alpha,\delta)\,\hat{\tilde{p}}(j_1,j_2), \tag{2.32}$$

$$\begin{aligned} &\hat{W}_2(j_1,j_2,\rho_\alpha,\delta) = \left(1+\frac{\delta^2}{(\rho_\alpha(j_1,j_2))^2-\delta^2}\right)^{-1} \quad \text{for} \quad (\rho_\alpha(j_1,j_2))^2-\delta^2>0, \\ &\hat{W}_2(j_1,j_2,\rho_\alpha,\delta) = 0 \quad \text{for} \quad (\rho_\alpha(j_1,j_2))^2-\delta^2\le 0, \end{aligned} \tag{2.33}$$

where $(j_1,j_2)\in\hat{I}_{n_s,n_\varphi}$; in addition, $\delta = \delta(p,\tilde{p},\alpha,\varepsilon_2)$ is determined from the equation

$$\zeta(p, W_2(\rho_\alpha,\delta)\,\tilde{p},\Gamma) = \varepsilon_2\zeta_{appr}(p), \tag{2.34}$$

where $\zeta_{appr}(p)$ is defined by (2.23). We emphasize that, although W_2 is applied to $\tilde{p}$, δ of (2.33), (2.34) depends not only on $\tilde{p}$, α and ε_2, but also on p. One can see that $\hat{W}_2$ suppresses $\hat{\tilde{p}}$ in the frequency region, where ρ_α^2 is small in comparison with δ^2. Our algorithm for finding δ from (2.34) is based on the bisection method and is, actually, similar to the related algorithm of Section 6 of [GN] (which was mentioned already in connection with equation (2.18) for ω).

2.3. *Additional remarks on the two-step filtration W_2W_1.* Note that in our numerical examples we obtained that our two-step filtration (1.5)-(1.7) gives the best result $\tilde{\tilde{p}} = W_2W_1p$ in the sense of the relative error $\zeta(\tilde{\tilde{p}}, g, \Gamma)$, where ζ is defined by (2.4) and g is the noiseless data of (1.4), if (actually) $\varepsilon_1 = 1$ and ε_2 is slightly smaller or equal to 1 in (2.18), (2.34).

Note also that for the case when $\varepsilon_1 = 0$ (or more precisely $W_1p = p$), G in (2.29) is defined by

$$\begin{aligned} &G(j_1, j_2, \alpha) = 0 \quad \text{if} \quad j_1 \neq 0, \\ &G(j_1, j_2, \alpha) = 1/n_\varphi \quad \text{if} \quad j_1 = 0, \end{aligned} \tag{2.35}$$

and δ^2 in (2.33) is defined by

$$\delta^2 = \sum_{\gamma \in \Gamma} p(\gamma), \tag{2.36}$$

our two-step filtration (1.5)-(1.7) is reduced to a filtration which is (more or less) similar to one given in [BCB] (and which was mentioned in [C]).

3. Reconstruction of Cf from CP_af and a

First, we consider the following explicit inversion formula

$$Cf = \mathcal{N}_a g, \tag{3.1}$$

where $g = CP_af$,

$$\mathcal{N}_a q(x) = \frac{1}{4\pi}\left(-\frac{\partial}{\partial x_1}\int\limits_{\mathbb{S}^1} K(x,\theta)\theta_2 d\theta + \frac{\partial}{\partial x_2}\int\limits_{\mathbb{S}^1} K(x,\theta)\theta_1 d\theta\right), \tag{3.2a}$$

$$K(x,\theta) = \exp\left[-\mathcal{D}a(x,-\theta)\right]\tilde{q}_\theta(x\theta^\perp), \tag{3.2b}$$

$$\begin{aligned} &\tilde{q}_\theta(s) = \exp\big(A_\theta(s)\big)\cos\big(B_\theta(s)\big)\, H\big(\exp\left(A_\theta\right)\cos\left(B_\theta\right) q_\theta\big)(s) + \\ &\exp\big(A_\theta(s)\big)\sin\big(B_\theta(s)\big)\, H\big(\exp\left(A_\theta\right)\sin\left(B_\theta\right) q_\theta\big)(s), \end{aligned} \tag{3.2c}$$

$$A_\theta(s) = \frac{1}{2}Pa(s,\theta), \quad B_\theta(s) = H\, A_\theta(s), \quad q_\theta(s) = q(s,\theta), \tag{3.2d}$$

where q is a test function, $P = P_0$ is the classical two-dimensional ray transformation (i.e. P_0 is defined by (1.1a) with $a \equiv 0$), H is the Hilbert transformation defined by the formula

$$H\, u(s) = \frac{1}{\pi}\, p.v. \int\limits_{\mathbb{R}} \frac{u(t)}{s-t} dt, \tag{3.3}$$

where u is a test function, $x = (x_1, x_2) \in \mathbb{R}^2$, $\theta = (\theta_1, \theta_2) \in \mathbb{S}^1$, $\theta^\perp = (-\theta_2, \theta_1)$, $s \in \mathbb{R}$, $d\theta$ is arc-length measure on the circle $\mathbb{S}^1$.

In a slightly different form (using complex notations) formula (3.1) was obtained in [No]. Some new proofs of this formula were given in [Na] and [BS]. Formula (3.1) was successfully implemented numerically in [Ku] and [Na] via a direct generalization of the (classical) filtered back-projection (FBP) algorithm. However, this generalized FBP algorithm turned out to be less stable, in general, than its classical analogue. Some possibilities for improving the stability of SPECT imaging based on (3.1), (3.2) with respect to the Poisson noise in the emission data g were proposed, in particular, in [Ku] (preprint version), [GJKNT] and [GN]. Some fast numerical implementation of formula (3.1) was proposed in [BM].

Second, assuming (1.2), we consider the iterative reconstruction method with the following step. If Cf_n is an approximation with the number n to Cf, where $g = CP_af$, then we

(1) compute

$$h_n(s,\theta) = (g(s,\theta) + \mu_n)\frac{PCf_n(s,\theta) + \mu_n}{P_aCf_n(s,\theta) + \mu_n} - \mu_n, \tag{3.4}$$

where μ_n is some sufficiently small positive constant depending on P_aCf_n such that $P_aCf_n(s,\theta) + \mu_n > 0$ for $(s,\theta) \in \mathbb{R} \times \mathbb{S}^1$, $P = P_0$ is defined by (1.1a) with $a \equiv 0$

and (2) compute

$$Cf_{n+1} = P^{-1}h_n \tag{3.5}$$

using (3.1) with $a \equiv 0$ (i.e. using a variant of the classical FBP algorithm). This step (i.e. the passage from Cf_n to Cf_{n+1} via (3.4), (3.5)) is a variation of the step of the iterative SPECT reconstruction algorithm of [MNOY] (see also [MIMIKIH] and [GJKNT]). This algorithm (with the step (3.4), (3.5)) is rather stable or, more precisely, its stability properties with respect to the Poisson noise in the emission data g are comparable with the stability properties of (3.1) for $a \equiv 0$ (i.e. with the stability properties of the classical FBP algorithm).

In the present work we improve the stability of SPECT reconstruction based on (3.1), (3.2) or/and on (3.4), (3.5) with respect to the Poisson noise in the emission data g by means of our data dependent filtrations (1.5)-(1.7) mentioned in the introduction and presented in detail in Section 2.

Actually, in the present work (in a similar way with [Ku] (preprint version) and [GJKNT]) we consider, mainly, the reconstructions Cf_1 and Cf_2, where Cf_1 is reconstructed via (3.1), (3.2) and Cf_2 is obtained proceeding from Cf_1 via (3.4)-(3.5). This can be considered as a stabilization of (3.1) or as an acceleration of the iterative reconstruction based on (3.4), (3.5).

4. Numerical examples

4.0. *Preliminary remarks.* To illustrate our (emission) data dependent filtrations (1.5)-(1.7) mentioned in the introduction, presented in detail in Section 2 (and extended also for some cases on the attenuation map), we consider two well-known SPECT phantom

(elliptical chest phantom and Utah phantom). Further, for each of these phantoms the attenuation map a and the emitter activity f (and all reconstructions of f) are considered on

$$X = \{x_{i,j} : \ x_{i,j} = (-R + (i-1)\Delta s, -R + (j-1)\Delta s), \\ \Delta s = 2R/(n_s - 1), \quad i = 1, \dots, n_s, \ j = 1, \dots, n_s\}, \tag{4.1}$$

the attenuated ray transform $g = CP_a f$ and the noisy emission data p (and all filtrations of p) are considered on Γ defined by (1.3), where R of (4.1) and (1.3) is the radius of image support of (1.2) and $n_s = 128$, $n_\varphi = 128$ in (4.1), (1.3); in addition the 2D discrete Fourier transform Fq is considered on $\hat{I}_{n_s,n_\varphi}$ defined by (2.7) for any q on Γ. In addition to (2.3), (2.4), we use also the following notations

$$\xi(u, v, X) = \frac{\|u - v\|_{L^2(X)}}{\|v\|_{L^2(X)}}, \tag{4.2}$$

$$\|w\|_{L^2(X)} = \Delta s \big(\sum_{x \in X} |w(x)|^2 \big)^{1/2}, \tag{4.3}$$

where u, v, w are functions on X.

Given f and a on X, we assume that $P_a f$ is defined on Γ and is the numerical realization of (1.1) as in [Ku]. Given a on X and q on Γ, we assume that $\mathcal{N}_a q$ is defined on X and denote the numerical realization of (3.2) as in [Ku], [Na] without any regularization. Given Cf_1 and a on X and g on Γ, we assume that $Cf_m(Cf_1, a, g)$ is defined on X and is obtained numerically proceeding from Cf_1 via (3.4), (3.5) by $m - 1$ steps without any regularization in (3.5) (here we do not assume that $g = CP_a f$).

Notice that all two-dimensional images of the present work, except the spectrum of projections, are drawn using a linear greyscale, in such a way that the dark grey color represents zero (or negative values, if any) and white corresponds to the maximum value of the imaged function. For the spectrum of projections, a non-linear greyscale was used, because of too great values of the spectrum for small frequencies.

4.1. *Elliptical chest phantom.* We consider a version of the elliptical chest phantom (used for numerical simulations of cardiac SPECT imaging; see [HL], [Br], [GN]). The major axis of the ellipse representing the body is 30 cm. This phantom is referred further as phantom 1.

The attenuation map for phantom 1 is shown in figure 1(a); the attenuation coefficient a is 0.04 cm^{-1} in the lung regions (modeled as two interior ellipses), 0.15 cm^{-1} elsewhere within the body ellipse, and zero outside the body.

The emitter activity f for phantom 1 is shown in figure 1(b); f is in the ratio 8:0:1:0 in myocardium (represented as a ring), lungs, elsewhere within the body, and outside the body.

The attenuated ray transform $g = CP_a f$ and noisy emission data p of (1.4) for phantom 1 are shown in figures 2(a), 3(a). In addition, the constant C was specified in order to have that the noise level $\zeta(p, g, \Gamma) \approx 0.3$ (where ζ is defined by (2.4)). Actually, we have that

$$\zeta(p, g, \Gamma) = 0.298, \ \zeta_{appr}(p) = 0.3 \tag{4.4}$$

for phantom 1. Figures 2(b), 3(b) show the spectrum $|Fg|$, $|Fp|$ for phantom 1.

Figures 4(a),(b) show for phantom 1 our basic space invariant data dependent filtration $\bar{p} = W(\omega)p$, $\omega = \omega(p, \varepsilon_1)$, $\varepsilon_1 = 0.98$, proposed in [GN] and the spectrum $|F\bar{p}|$, where $W(\omega)p$, $\omega = \omega(p, \varepsilon_1)$ are defined by (2.17), (2.18) for the case (2.19). We have that

$$\zeta(\bar{p}, g, \Gamma) = 0.103, \ \zeta(p, \bar{p}, \Gamma) = 0.294. \tag{4.5}$$

Figures 5(a),(b) show for phantom 1 the space variant data dependent filtration $\tilde{p} = W_1 p$ developed in the present work and the spectrum $|F\tilde{p}|$ where $W_1 p$ is defined by (2.21) for $l = m = 8$, $\varepsilon_1 = 1$. We have that

$$\zeta(\tilde{p}, g, \Gamma) = 0.089, \quad \zeta(p, \tilde{p}, \Gamma) = 0.278. \tag{4.6}$$

Formulas (4.5), (4.6) show that $\tilde{p} = W_1 p$ is better than its space invariant prototype $\bar{p} = W(\omega)p$, at least, in the sense of the relative error in $L^2(\Gamma)$ with respect to the noiseless data g. In addition, figures 2(b), 4(b) and 5(b) show that $|F\tilde{p}|$ looks more similar to $|Fg|$ than $|F\bar{p}|$. Note also that figure 5(c) shows for phantom 1 the function ρ_α defined by (2.29), (2.30), where $\tilde{p} = W_1 p$, $\alpha = 0.5$, $n = 5$.

Figure 6(a) shows for phantom 1 our two-step filtration $\tilde{\tilde{p}} = W_2 W_1 p$ mentioned in (1.5)-(1.7) and defined precisely by (2.31)-(2.34), where $\tilde{p} = W_1 p$ is defined as for figure 5(a) and further $\alpha = 0.5$, $n = 5$, $\varepsilon_2 = 0.97$. We have that

$$\zeta(\tilde{\tilde{p}}, g, \Gamma) = 0.080, \quad \zeta(p, \tilde{\tilde{p}}, \Gamma) = 0.294. \tag{4.7}$$

Formulas (4.6), (4.7) show that $\tilde{\tilde{p}} = W_2 W_1 p$ is better than $\tilde{p} = W_1 p$ in the sense of the relative error in $L^2(\Gamma)$ with respect to the noiseless data g. Figure 6(b) shows the spectrum $|F\tilde{\tilde{p}}|$. Note that $|F\tilde{\tilde{p}}|$ looks more or less similar to $|F\tilde{p}|$ in figures 5(b), 6(b). To explain the principal difference between $|F\tilde{\tilde{p}}|$ and $|F\tilde{p}|$ we use figures 7(a)-(c) showing the profiles of $|Fg|$, $|F\tilde{p}|$ and $|F\tilde{\tilde{p}}|$ for $j_2 = 32$. Figures 7(b),(c) show that, actually, $supp\, F\tilde{\tilde{p}}$ is considerably more localized around the center (0,0) of $\hat{I}_{n_s, n_\varphi}$ than $supp\, F\tilde{p}$. One can not see it properly from figures 5(b), 6(b), because the values $|F\tilde{p}(j_1, j_2)|$ are already very small for $j_2 = 32$ in comparison with $|F\tilde{p}(j_1, j_2)|$ for some (j_1, j_2) more close to the centerer (0,0).

Figures 8(a)-(c) show for phantom 1 the reconstructions

$$Cf_1^0 = \mathcal{N}_a g, \quad Cf_2^0 = Cf_2(Cf_1^0, a, g) \ \text{ for } \ g = CP_a f \tag{4.8}$$

(see definitions given in subsection 4.0), and the profile of Cf_2^0 for $j = 64$.

Figures 9(a)-(c) show for phantom 1 the reconstructions

$$Cf_1 = \mathcal{N}_a p, \quad Cf_2 = Cf_2(Cf_1, a, p), \tag{4.9}$$

and the profile of Cf_2 for $j = 64$, where p is the noisy emission data (shown in figure 3(a)). We have that

$$\xi(Cf_1, Cf_1^0, X) = 1.576, \quad \xi(Cf_2, Cf_2^0, X) = 0.849, \tag{4.10}$$

where Cf_1^0, Cf_2^0 are defined by (4.8), Cf_1, Cf_2 are defined by (4.9) (and ξ is defined by (4.2)).

Figures 10(a)-(c) show for phantom 1 the reconstructions

$$Cf_1 = \mathcal{N}_a\bar{p}, \quad Cf_2 = Cf_2(Cf_1, a, \bar{p}), \tag{4.11}$$

and the profile of Cf_2 for $j = 64$, where $\bar{p}$ is our basic space invariant data dependent filtration (shown in figure 4(a)). We have that

$$\xi(Cf_1, Cf_1^0, X) = 0.376, \quad \xi(Cf_2, Cf_2^0, X) = 0.308, \tag{4.12}$$

where Cf_1^0, Cf_2^0, Cf_1, Cf_2 are defined by (4.8), (4.11).

Figures 11(a)-(c) show for phantom 1 the reconstructions

$$Cf_1 = \mathcal{N}_a\tilde{p}, \quad Cf_2 = Cf_2(Cf_1, a, \tilde{p}), \tag{4.13}$$

and the profile of Cf_2 for $j = 64$, where $\tilde{p} = W_1 p$ is our space invariant data dependent filtration (shown in figure 5(a)). We have that

$$\xi(Cf_1, Cf_1^0, X) = 0.404, \quad \xi(Cf_2, Cf_2^0, X) = 0.280, \tag{4.14}$$

where Cf_1^0, Cf_2^0, Cf_1, Cf_2 are defined by (4.8), (4.13).

Figures 12(a)-(c) show for phantom 1 the reconstructions

$$Cf_1 = \mathcal{N}_a\tilde{\tilde{p}}, \quad Cf_2 = Cf_2(Cf_1, a, \tilde{\tilde{p}}), \tag{4.15}$$

and the profile of Cf_2 for $j = 64$, where $\tilde{\tilde{p}} = W_1 p$ is our two-step space invariant data dependent filtration (shown in figure 6(a)). We have that

$$\xi(Cf_1, Cf_1^0, X) = 0.329, \quad \xi(Cf_2, Cf_2^0, X) = 0.258, \tag{4.16}$$

where Cf_1^0, Cf_2^0, Cf_1, Cf_2 are defined by (4.8), (4.15).

Figures 10, 11 show that the reconstructions (4.13) (using the space variant data dependent filtration $p \to \tilde{p}$) give a higher resolution in the "myocardium" region than the reconstructions (4.11) (using the space invariant data dependent filtration $p \to \bar{p}$). However, in spite of the property that $\zeta(\tilde{p}, g, \Gamma) < \zeta(\bar{p}, g, \Gamma)$ (see (4.5), (4.6)), we have that Cf_1 of (4.13) is even worse than Cf_1 of (4.11) in the sense of the relative error in $L^2(X)$ with respect to Cf_1^0 of (4.8) (see (4.12), (4.14)). The reason is that $supp\, F\tilde{p}$ is less localized around the center (0,0) of $\hat{I}_{n_s,n_\varphi}$ than $supp\, F\bar{p}$ and that $\mathcal{N}_a q$ is not very stable with respect to high frequency harmonics of q for $a \not\equiv 0$.

Figures 10, 12 and formulas (4.12), (4.16) show that the reconstructions (4.15) (using the two-step space variant data dependent filtration $p \to \tilde{\tilde{p}}$) are considerably better than the reconstructions of (4.11) (using the space invariant data dependent filtration $p \to \bar{p}$) in the sense of the relative errors in $L^2(X)$ with respect to the noiseless reconstructions of (4.8). However, the reconstructions (4.15) have only a slightly higher resolution in the "myocardium" region than the reconstructions (4.11). Actually, the resolution in

important regions is a very important parameter in SPECT imaging. Therefore, we present below some additional reconstructions on phantom 1.

Figure 13(a),(b) show for phantom 1 the reconstruction

$$Cf_2 = Cf_2(Cf_1, a, \tilde{p}), \quad \text{where} \quad Cf_1 = \mathcal{N}_a\tilde{\tilde{p}}, \tag{4.17}$$

and its profile for $j = 64$. One can see that we use in (4.17) the both aforementioned filtrations $\tilde{p}$ and $\tilde{\tilde{p}}$ (shown in figures 5(a), 6(a)). We have that

$$\xi(Cf_2, Cf_2^0, X) = 0.254, \tag{4.18}$$

where Cf_2^0, Cf_2 are defined in (4.8), (4.17). Note that Cf_2 of (4.17) is the best among the reconstructions Cf_2 (from p and its filtrations) given in this paper for phantom 1 in the sense of the relative error in $L^2(X)$ with respect to Cf_2^0 of (4.8). This Cf_2 of (4.17) contains considerably less artifacts than Cf_2 of (4.13). The reason is that the first approximation $Cf_1 = \mathcal{N}_a\tilde{\tilde{p}}$ of (4.15), (4.17) is (roughly speaking) better than the first approximation $Cf_1 = \mathcal{N}_a\tilde{p}$ of (4.13) and that $Cf_2(Cf_1, a, q)$ is sufficiently stable with respect to high frequency harmonics of q. In addition, the resolution of Cf_2 of (4.17) in the "myocardium" region is similar to the resolution of Cf_2 of (4.13) in this region and is noticeably greater than such a resolution for Cf_2 of (4.11). The reason is that Cf_2 of (4.17) as well as Cf_2 of (4.13) uses $\tilde{p}$.

Figure 14(a),(b) show for phantom 1 the reconstruction

$$Cf_2 = Cf_2(Cf_1, a, p'), \quad \text{where} \quad Cf_1 = \mathcal{N}_a\tilde{\tilde{p}}, \tag{4.19}$$

and its profile for $j = 64$, where Cf_1 is the same as in (4.15), (4.17) and $p' = W_1p$ with W_1p defined by (2.21) for $l = m = 8$ and $\varepsilon_1 = 0.8$ (instead of $\varepsilon_1 = 1$ used for $\tilde{p}$). We have that

$$\zeta(p', g, \Gamma) = 0.123, \quad \zeta(p, p', \Gamma) = 0.229, \tag{4.20}$$

$$\xi(Cf_2, Cf_2^0, X) = 0.285, \tag{4.21}$$

where Cf_2^0, Cf_2 are defined in (4.8), (4.19). Note that Cf_2 of (4.19) is the best among the reconstructions Cf_2 (from p and its filtrations) given in this paper for phantom 1 in the sense of the balance between the resolution in the "myocardium" region and the relative error in $L^2(X)$ with respect to Cf_2^0 of (4.8).

4.2. *Utah phantom.* As it was mentioned already in the introduction, if the attenuation map a is strongly nonuniform in a neighborhood of the region where the emitter activity f is of particular interest, then to reconstruct Cf properly it may be important to smooth a in a consistent way with filtering p. To illustrate it we consider a simulated numerical version of the so called Utah phantom (designed at the 2^{nd} International Meeting on fully Three-Dimensional Image Reconstruction in Radiology and Nuclear Medicine, Snowbird, Utah, 1993). A real non simulated version of this phantom was considered, in particular, in [GJKNT]. However, in the present paper we consider its simulated numerical version in

order to present the effect of aforementioned smoothing a more rigorously. This simulated version is referred further as phantom 2.

Geometrically, phantom 2 consists of a large disk containing two small disks. The radius of the large disk is 10 cm. The attenuation map a and the emitter activity f for phantom 2 are shown in figures 15(a),(b). The attenuation coefficient a is 0.16 cm^{-1} in the large disk outside the small disks, 0.63 cm^{-1} in the left small disk, 0.31 cm^{-1} in the right small disk, and zero outside the large disk. The function f is a positive constant in the large disk outside the small disks and zero elsewhere. The attenuation ray transform $g = CP_a f$ for phantom 2 is shown in figure 15(c).

Figure 16(a) shows for phantom 2 noisy emission data p of (1.4). In addition, the constant C was specified in order to have that the noise level $\zeta(p, g, \Gamma) \approx 0.23$. Actually, we have that

$$\zeta(p, g, \Gamma) = 0.23, \quad \zeta_{appr}(p) = 0.23 \tag{4.22}$$

for phantom 2. Figures 16(b) and (c) show for phantom 2 the filtrations $\tilde{p} = W_1 p$ and $\tilde{\tilde{p}} = W_2 W_1 p$ defined by (2.21) for $\varepsilon_1 = 1$ and (2.31)-(2.34) for $\alpha = 0.5$, $n = 5$, $\varepsilon_2 = 0.98$. We have that

$$\zeta(\tilde{p}, g, \Gamma) = 0.061, \quad \zeta(p, \tilde{p}, \Gamma) = 0.211, \tag{4.23}$$

$$\zeta(\tilde{\tilde{p}}, g, \Gamma) = 0.047, \quad \zeta(p, \tilde{\tilde{p}}, \Gamma) = 0.225. \tag{4.24}$$

Figures 17(a)-(c) show for phantom 2 the reconstructions

$$Cf_1 = \mathcal{N}_a p, \quad Cf_2 = Cf_2(Cf_1, a, p) \tag{4.25}$$

and the profile of Cf_2 for $j = 64$, where p is the noisy emission data shown in figure 16(a). We have that

$$\xi(Cf_1, Cf_1^0, X) = 3.40, \quad \xi(Cf_2, Cf_2^0, X) = 1.643, \tag{4.26}$$

where Cf_1, Cf_2 are defined by (4.25) and

$$Cf_1^0 = \mathcal{N}_a g, \quad Cf_2^0 = Cf_2(Cf_1^0, a, g) \tag{4.27}$$

are the reconstructions from the noiseless data g shown in figure 15(c). (To reduce the number of figures given in this paper we do not show the reconstructions Cf_1^0 and Cf_2^0 for phantom 2.)

Figures 18(a)-(c) show for phantom 2 the reconstructions

$$Cf_1 = \mathcal{N}_a \tilde{p}, \quad Cf_2 = Cf_2(Cf_1, a, \tilde{p}) \tag{4.28}$$

and the profile of Cf_2 for $j = 64$, where $\tilde{p} = W_1 p$ is shown in figure 16(b). We have that

$$\xi(Cf_1, Cf_1^0, X) = 0.593, \quad \xi(Cf_2, Cf_2^0, X) = 0.300, \tag{4.29}$$

where Cf_1^0, Cf_2^0, Cf_1, Cf_2 are defined by (4.27), (4.28).

Figures 19(a)-(c) show for phantom 2 the reconstructions

$$Cf_1 = \mathcal{N}_{\tilde{a}}\tilde{p}, \quad Cf_2 = Cf_2(Cf_1, \tilde{a}, \tilde{p}) \tag{4.30}$$

and the profile of Cf_2 for $j = 64$, where $\tilde{p} = W_1 p$ is shown in figure 16(b) and $\tilde{a}$ is a smoothed consistently with the filtration $p \to \tilde{p}$ according to (1.8), (1.9). We have that

$$\xi(Cf_1, Cf_1^0, X) = 0.523, \quad \xi(Cf_2, Cf_2^0, X) = 0.236, \tag{4.31}$$

where Cf_1^0, Cf_2^0, Cf_1, Cf_2 are defined by (4.27), (4.30). Figures 18, 19 and formulas (4.29), (4.31) show that Cf_2 of (4.30) using the filtration $p \to \tilde{p}$ and consistent smoothing $a \to \tilde{a}$ is considerably better than Cf_2 of (4.28) which also uses the filtration $p \to \tilde{p}$ but does not use any smoothing a.

Note that (to our experience) the stability of $Cf_n(\mathcal{N}_a p, a, p)$ increases, in general, when n increases. Therefore, to illustrate more the efficiency of our filtration $p \to \tilde{p}$ for Cf_n with $n \geq 2$ and possible importance of consistent smoothing $a \to \tilde{a}$ we show on figures 20 (a)-(c), 21 (a)-(c) the reconstructions $Cf_4(\mathcal{N}_a p, a, p)$, $Cf_4(\mathcal{N}_a \tilde{p}, a, \tilde{p})$, $Cf_4(\mathcal{N}_{\tilde{a}} \tilde{p}, \tilde{a}, \tilde{p})$ for phantom 2 and their profiles for $j = 64$ (where $\mathcal{N}_a p$, $\mathcal{N}_a \tilde{p}$, $\mathcal{N}_{\tilde{a}} \tilde{p}$ are shown on figures 17(a), 18(a), 19(a)).

(a) (b)

Figure 1. Attenuation map a (a) and emitter activity f (b) for phantom 1.

(a) (b)

Figure 2. Noiseless emission data $g = CP_a f$ (a) and the spectrum $|Fg|$ (b) for phantom 1.

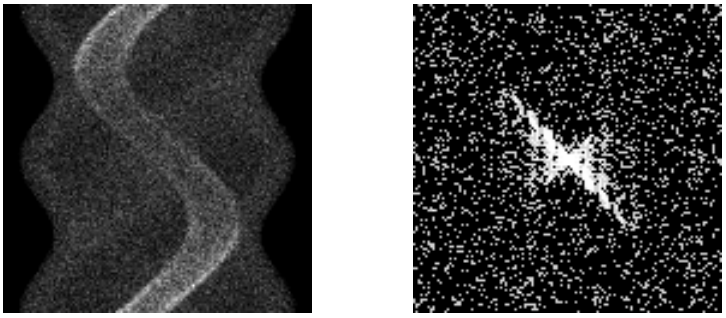

(a) (b)

Figure 3. Noisy emission data p (a) and the spectrum $|Fp|$ (b) for phantom 1.

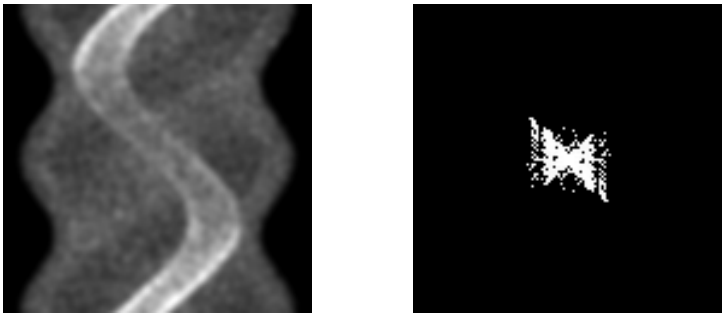

(a) (b)

Figure 4. Space invariant data dependent filtration $\bar{p} = W(\omega(p, \varepsilon_1))p$, $\varepsilon_1 = 0.98$, of [GN] (a) and its spectrum $|F\bar{p}|$ (b) for phantom 1.

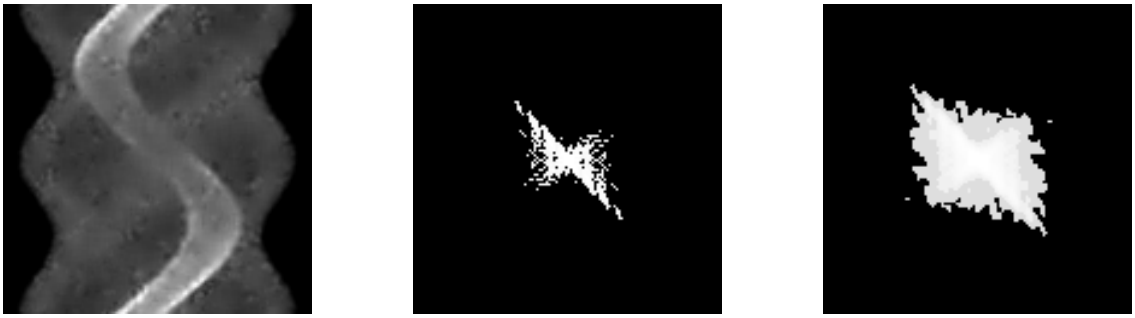

(a) (b) (c)

Figure 5. Space variant data dependent filtration $\tilde{p} = W_1 p$ of (1.5), (1.6), (2.21) with $\varepsilon_1 = 1$, $l = m = 8$ (a), its spectrum $|F\tilde{p}|$ (b), and its smoothed spectrum ρ_α of (2.29), (2.30) with $\alpha = 0.5$, $n = 5$ (c) for phantom 1.

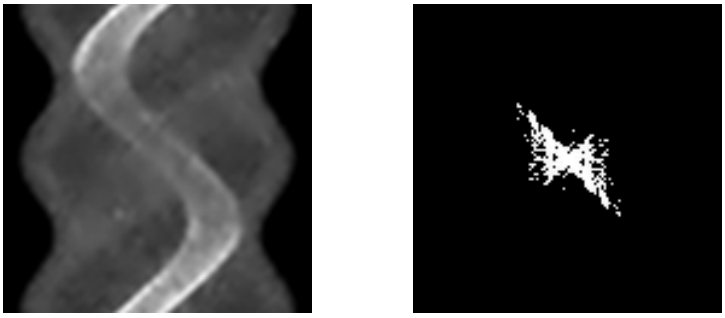

(a) (b)

Figure 6. Two-step space variant data dependent filtration $\tilde{\tilde{p}} = W_2 W_1 p$ of (1.5)-(1.7), (2.21), (2.31)-(2.34) with $\varepsilon_1 = 1$, $l = m = 8$, $\alpha = 0.5$, $n = 5$, $\varepsilon_2 = 0.97$ (a) and its spectrum $|F\tilde{\tilde{p}}|$ (b) for phantom 1.

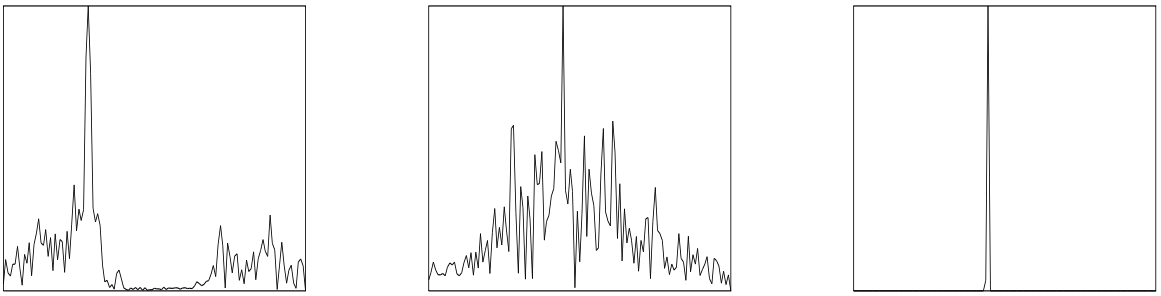

(a) (b) (c)

Figure 7. Profiles $|Fg(\cdot, 32)|$ (a), $|F\tilde{p}(\cdot, 32)|$ (b), and $|F\tilde{\tilde{p}}(\cdot, 32)|$ (c) of the images shown in Figures 2(b), 5(b), 6(b). The maximum values of these profiles are in the ratio $1 : 0.72 : 0.087$ for the cases (a), (b), (c), respectively.

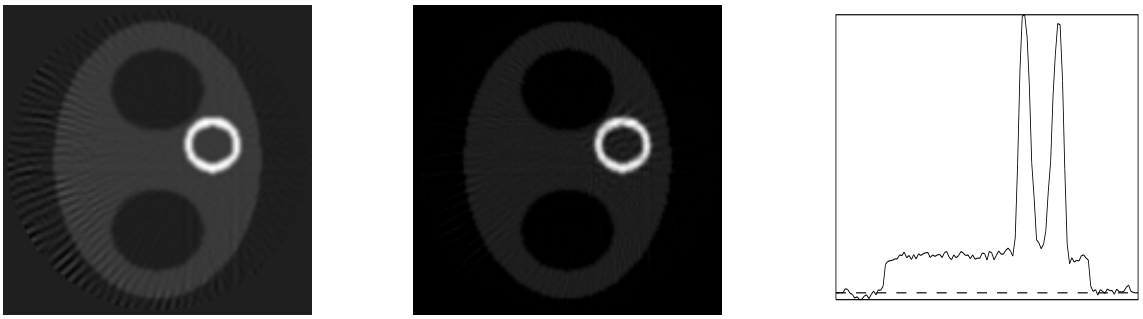

(a) (b) (c)

Figure 8. Reconstructions $Cf_1^0 = \mathcal{N}_a g$ (a), $Cf_2^0 = Cf_2(Cf_1^0, a, g)$ (b) from the noise-

less emission data g, and the profile of Cf_2^0 for $j = 64$ (c) for phantom 1.

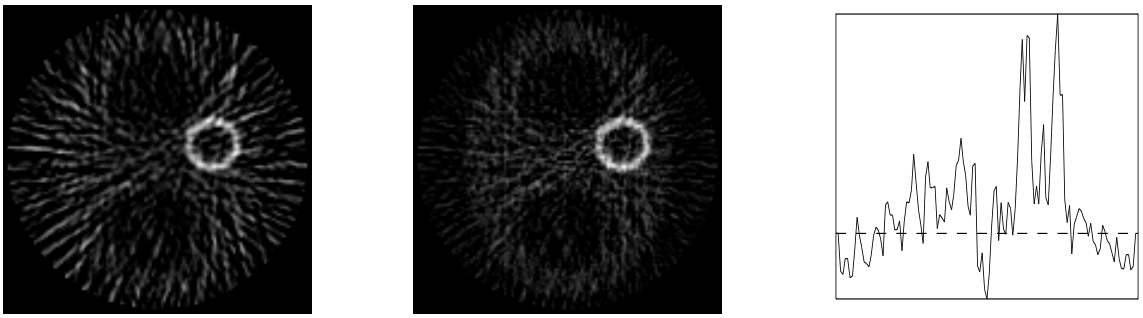

(a) (b) (c)

Figure 9. Reconstructions $Cf_1 = \mathcal{N}_a p$ (a), $Cf_2 = Cf_2(Cf_1, a, p)$ (b) from the noisy emission data p without any filtration, and the profile of Cf_2 for $j = 64$ (c) for phantom 1.

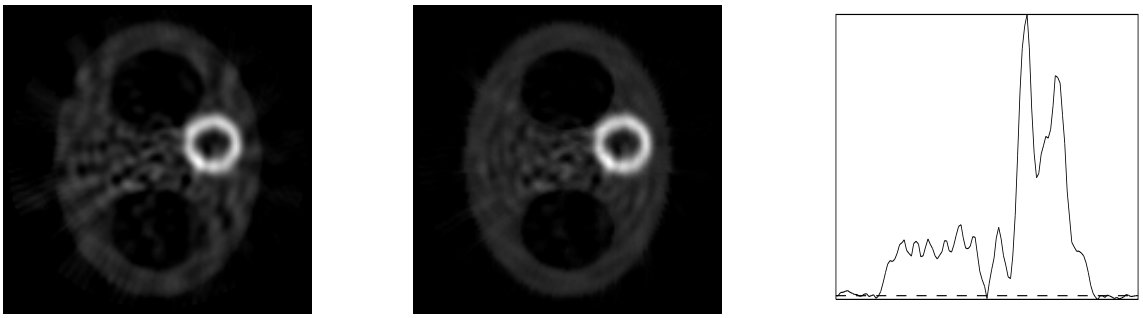

(a) (b) (c)

Figure 10. Reconstructions $Cf_1 = \mathcal{N}_a \bar{p}$ (a), $Cf_2 = Cf_2(Cf_1, a, \bar{p})$ (b), and the profile of Cf_2 for $j = 64$ (c) for phantom 1.

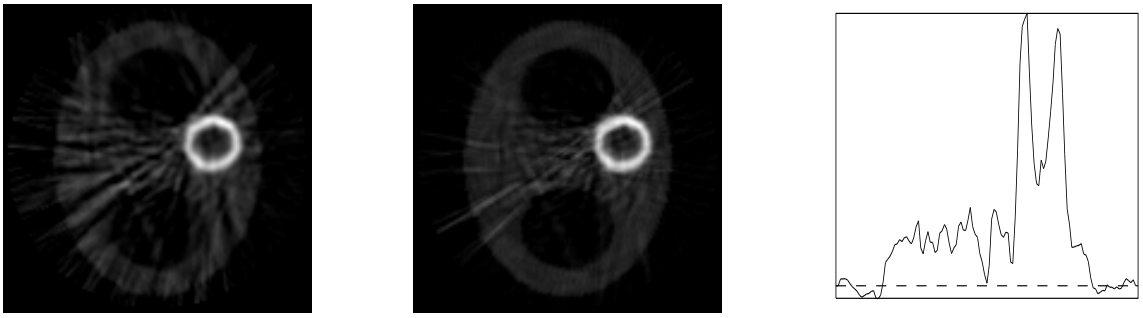

(a) (b) (c)

Figure 11. Reconstructions $Cf_1 = \mathcal{N}_a\tilde{p}$ (a), $Cf_2 = Cf_2(Cf_1, a, \tilde{p})$ (b), and the profile of Cf_2 for $j = 64$ (c) for phantom 1.

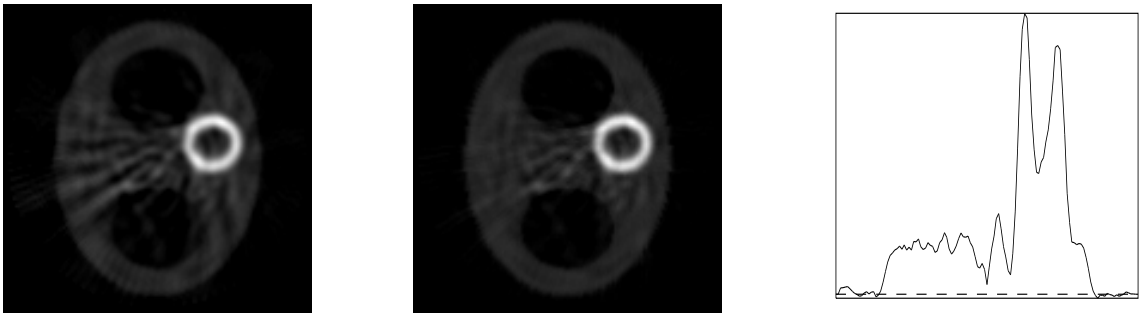

(a) (b) (c)

Figure 12. Reconstructions $Cf_1 = \mathcal{N}_a\tilde{\tilde{p}}$ (a), $Cf_2 = Cf_2(Cf_1, a, \tilde{\tilde{p}})$ (b), and the profile of Cf_2 for $j = 64$ (c) for phantom 1.

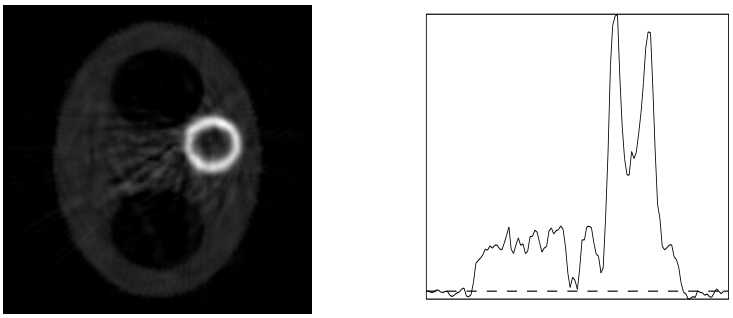

(a) (b)

Figure 13. Reconstruction $Cf_2 = Cf_2(\mathcal{N}_a\tilde{\tilde{p}}, a, \tilde{p})$ (a) and its profile for $j = 64$ (b) for phantom 1.

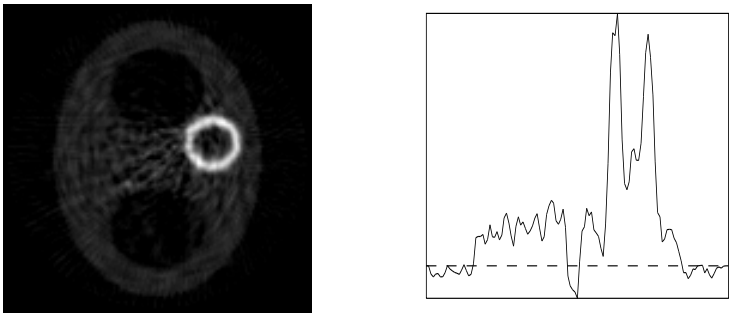

(a) (b)

Figure 14. Reconstruction $Cf_2 = Cf_2(\mathcal{N}_a\tilde{\tilde{p}}, a, p')$ (a) and its profile for $j = 64$ (b) for phantom 1.

(a) (b) (c)

Figure 15. Attenuation map a (a), emitter activity f (b), and noiseless emission data $g = CP_af$ (c) for phantom 2.

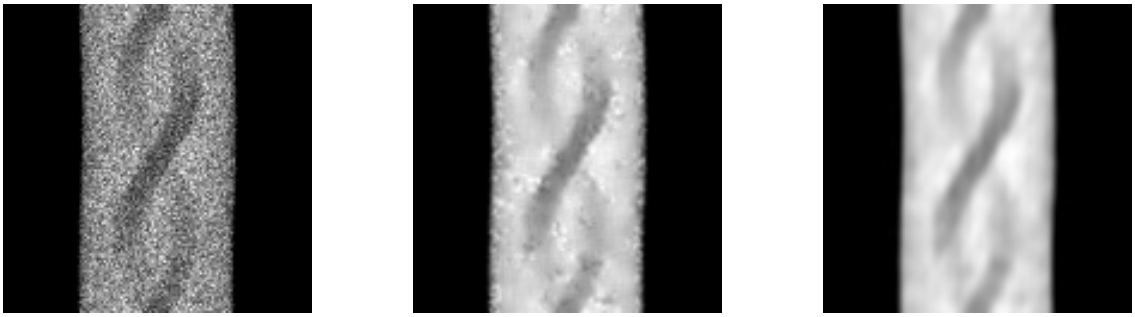

(a) (b) (c)

Figure 16. Noisy emission data p (a) and their filtrations $\tilde{p} = W_1p$ (b) and $\tilde{\tilde{p}} = W_2W_1p$ (c) of (1.5)-(1.7), (2.21), (2.31)-(2.34) with $\varepsilon_1 = 1$, $l = m = 8$, $\alpha = 0.5$, $n = 5$, $\varepsilon_2 = 0.98$ for phantom 2.

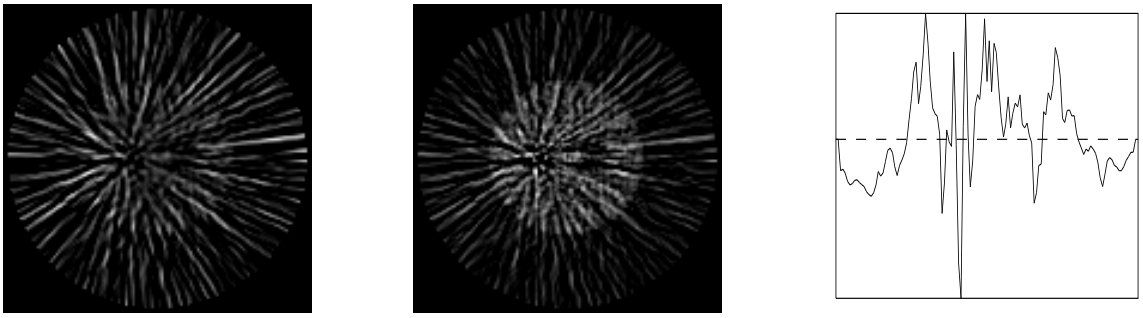

(a) (b) (c)

Figure 17. Reconstructions $Cf_1 = \mathcal{N}_a p$ (a), $Cf_2 = Cf_2(Cf_1, a, p)$ (b) from the noisy emission data p without any filtration and the profile of Cf_2 for $j = 64$ (c) for phantom 2.

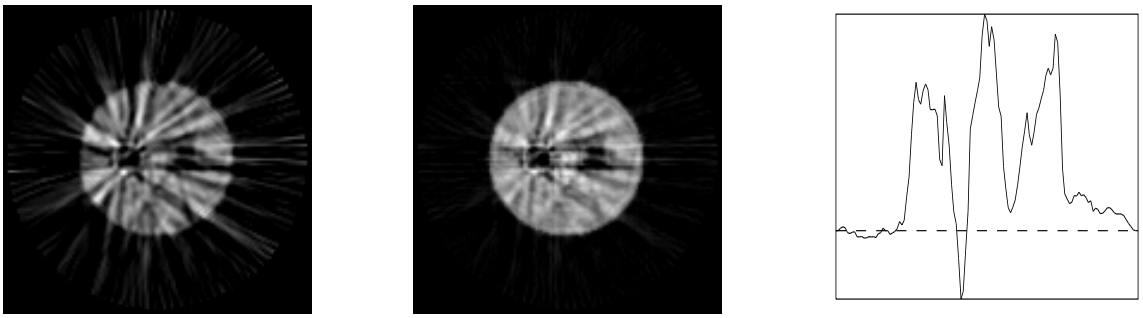

(a) (b) (c)

Figure 18. Reconstructions $Cf_1 = \mathcal{N}_a \tilde{p}$ (a), $Cf_2 = Cf_2(Cf_1, a, \tilde{p})$ (b) from the filtered emission data $\tilde{p}$ but without any smoothing a, and the profile of Cf_2 for $j = 64$ (c) for phantom 2.

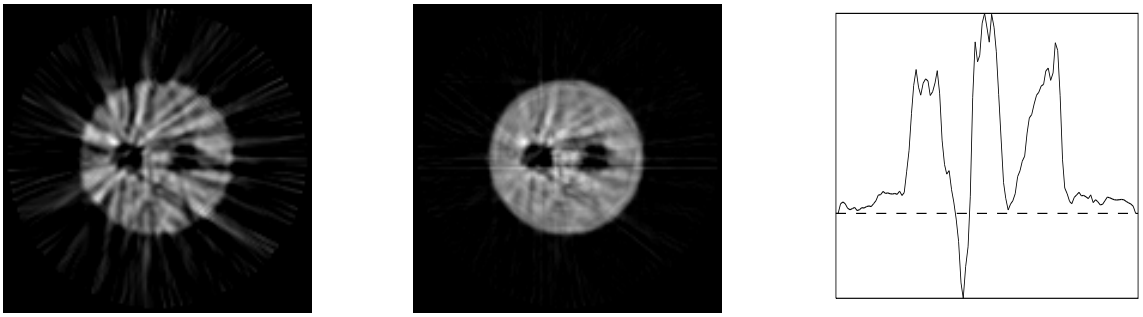

(a) (b) (c)

Figure 19. Reconstructions $Cf_1 = \mathcal{N}_{\tilde{a}} \tilde{p}$ (a), $Cf_2 = Cf_2(Cf_1, \tilde{a}, \tilde{p})$ (b) from the filtered emission data $\tilde{p}$ and with consistently smoothed attenuation map $\tilde{a}$, and the profile of Cf_2

for $j = 64$ (c) for phantom 2.

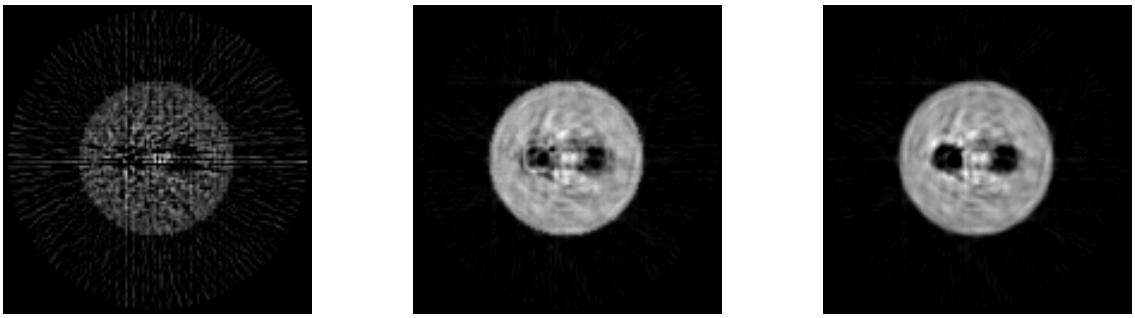

(a) (b) (c)

Figure 20. Reconstructions $Cf_4(\mathcal{N}_a p, a, p)$ (a), $Cf_4(\mathcal{N}_a \tilde{p}, a, \tilde{p})$ (b), and $Cf_4(\mathcal{N}_{\tilde{a}} \tilde{p}, \tilde{a}, \tilde{p})$ (c) for phantom 2.

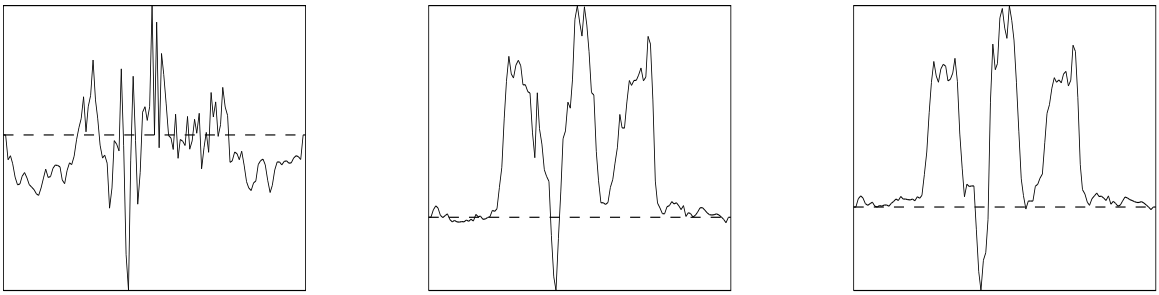

(a) (b) (c)

F Figure 21. Profiles $Cf_4(\mathcal{N}_a p, a, p)$ (a), $Cf_4(\mathcal{N}_a \tilde{p}, a, \tilde{p})$ (b), and $Cf_4(\mathcal{N}_{\tilde{a}} \tilde{p}, \tilde{a}, \tilde{p})$ (c) for $j = 64$ for phantom 2.

5. Conclusions

We proposed a two-step space variant data dependent filtration of the form (1.5)-(1.7) for SPECT emission data modeled as the 2D attenuated ray transformation with Poisson noise or, more precisely, as a function p of (1.4) on the detector set Γ defined by (1.3). The first step W_1 is, actually, a space variant version of the space invariant data dependent filtration developed in our recent work [GN]. The filtration W_1 is defined by formula (2.21) (and can be written in the form (1.6)). The second step W_2 is a space invariant filtration based on some results of [RL], [GB], [GouNol] and [GN]. The filtration W_2 is defined by (2.31)-(2.34) and depends on global spectral properties of p and $W_1 p$ (and can be written in the form (1.7)). For any our filtration W we strongly use the principle that the relative

error of p with respect to its filtration Wp should be commensurable (in a neighborhood of each point $\gamma \in \Gamma$ or globally on Γ) with the relative error of p with respect to the noiseless data g; in addition for the latter errors we use formulas (2.18b), (2.23).

To illustrate our filtrations we consider two well-known SPECT phantoms; see Section 4. More precisely, we consider a version of the elliptical chest phantom (this version is referred in the paper as phantom 1) and a simulated version of the so called Utah phantom (this version is referred in the paper as phantom 2). As regards the noise to signal ratio for the emission data p and their filtrations, we have, in particular, that

$$\zeta(p, g, \Gamma) = 0.298, \quad \zeta(\bar{p}, g, \Gamma) = 0.103,$$
$$\zeta(\tilde{p}, g, \Gamma) = 0.089, \quad \zeta(\tilde{\tilde{p}}, g, \Gamma) = 0.080,$$

for phantom 1 (see formulas (2.4), (4.4)-(4.7)) and

$$\zeta(p, g, \Gamma) = 0.23, \quad \zeta(\bar{p}, g, \Gamma) = 0.067,$$
$$\zeta(\tilde{p}, g, \Gamma) = 0.061, \quad \zeta(\tilde{\tilde{p}}, g, \Gamma) = 0.047,$$

for phantom 2 (see formulas (2.4), (4.22)-(4.24)), where $p \to \tilde{p} = W_1 p$ and $p \to \tilde{\tilde{p}} = W_2 W_1 p$ are the space variant data dependent filtrations of the present work and $p \to \bar{p}$ is our space invariant data dependent filtration of [GN]. One can see, in particular, that our two-step space variant filtration $p \to \tilde{\tilde{p}} = W_2 W_1 p$ reduces the initial ratio $\zeta(p, g, \Gamma) = 0.298$ to $\zeta(\tilde{\tilde{p}}, g, \Gamma) = 0.080$ for phantom 1 and the initial ratio $\zeta(p, g, \Gamma) = 0.23$ to $\zeta(\tilde{\tilde{p}}, g, \Gamma) = 0.047$ for phantom 2. One can see also that $\zeta(\tilde{\tilde{p}}, g, \Gamma)$ is noticeably smaller than $\zeta(\bar{p}, g, \Gamma)$ (22.3 per cent and 29.8 per cent of $\zeta(\bar{p}, g, \Gamma)$ smaller for phantom 1 and phantom 2 respectively).

As regards the relative error of the emitter activity reconstructed as Cf_1 (that is via (3.1), (3.2)) and Cf_2 (that is proceeding from Cf_1 and using also for stabilization (3.4), (3.5) for $n = 2$) with respect to the noiseless reconstructions $Cf_1^0 = \mathcal{N}_a g$ and $Cf_2^0 = Cf_2(\mathcal{N}_a g, a, g)$ (respectively) (see related definitions given in subsection 4.0), we have, in particular, that

$$\xi(\mathcal{N}_a p, Cf_1^0, X) = 1.576, \quad \xi(\mathcal{N}_a \bar{p}, Cf_1^0, X) = 0.376,$$
$$\xi(\mathcal{N}_a \tilde{p}, Cf_1^0, X) = 0.404, \quad \xi(\mathcal{N}_a \tilde{\tilde{p}}, Cf_1^0, X) = 0.329,$$

$$\xi(Cf_2(\mathcal{N}_a p, a, p), Cf_2^0, X) = 0.849, \quad \xi(Cf_2(\mathcal{N}_a \bar{p}, a, \bar{p}), Cf_2^0, X) = 0.308,$$
$$\xi(Cf_2(\mathcal{N}_a \tilde{p}, a, \tilde{p}), Cf_2^0, X) = 0.280, \quad \xi(Cf_2(\mathcal{N}_a \tilde{\tilde{p}}, a, \tilde{\tilde{p}}), Cf_2^0, X) = 0.258,$$
$$\xi(Cf_2(\mathcal{N}_a \tilde{\tilde{p}}, a, \tilde{p}), Cf_2^0, X) = 0.254,$$

for phantom 1 (see formulas (4.2), (4.10), (4.12), (4.14), (4.16), (4.18)) and

$$\xi(\mathcal{N}_a p, Cf_1^0, X) = 3.40, \quad \xi(\mathcal{N}_a \tilde{p}, Cf_1^0, X) = 0.59,$$
$$\xi(\mathcal{N}_{\tilde{a}} \tilde{p}, Cf_1^0, X) = 0.523,$$

$$\xi(Cf_2(\mathcal{N}_a p, a, p), Cf_2^0, X) = 1.63, \quad \xi(Cf_2(\mathcal{N}_a \tilde{p}, a, \tilde{p}), Cf_2^0, X) = 0.300,$$
$$\xi(Cf_2(\mathcal{N}_{\tilde{a}} \tilde{p}, \tilde{a}, \tilde{p}), Cf_2^0) = 0.236$$

for phantom 2 (see formulas (4.2), (4.26), (4.29)-(4.31)). These relative errors, figures 1, 8-15, 17-21 and the aforementioned (strong) initial noise to signal ratios of the emission data for our phantoms show an efficiency of the filtration methods developed in the present work in the framework of SPECT imaging based on FBP algorithms. (Note that for some of our reconstructions Cf_2 for phantom 1 (for example for $Cf_2 = Cf_2(\mathcal{N}_a\tilde{\tilde{p}}, a, \tilde{p})$) the relative error with respect to the noiseless reconstruction Cf_2^0 is even noticeably smaller than the noise to signal ratio of the initial emission data p.) In addition, one can see that:

(1) The reconstructions Cf_2 (based on (3.1), (3.2), (3.4)-(3.6), $n = 2$) are considerably more stable than Cf_1 (based on (3.1), (3.2)) (without precise relative errors in $L^2(X)$ it was observed earlier in [Ku] (preprint version) and [GJKNT]);

(2) Our two-step filtration $p \to \tilde{\tilde{p}} = W_2W_1p$ is especially efficient for the reconstructions Cf_1;

(3) A good first approximation Cf_1 is of course important for Cf_2 but on the stable step (3.4), (3.5) the simplified filtration $p \to \tilde{p} = W_1p$ may give even better result than (the complete one) $p \to \tilde{\tilde{p}} = W_2W_1p$. For example, $Cf_2(\mathcal{N}_a\tilde{\tilde{p}}, a, \tilde{p})$ is even better than $Cf_2(\mathcal{N}_a\tilde{\tilde{p}}, a, \tilde{\tilde{p}})$ for phantom 1 not only in the sense of the resolution in the "myocardium" region but also in the sense of the global relative error with respect to the noiseless reconstruction Cf_2^0;

(4) Above in these conclusions the filtration $p \to \tilde{p} = W_1p$ is considered with the parameter $\varepsilon_1 = 1$. To improve more the resolution of Cf_2 one can use on the step (3.4), (3.5) the filtration $p \to p'$ (that is our filtration $p \to \tilde{p}$ with decreased ε_1) only; see the reconstruction $Cf_2(\mathcal{N}_a\tilde{\tilde{p}}, a, p')$ shown in figure 14 for phantom 1.

(5) If the attenuation map a is strongly nonuniform in a neighborhood of a region where the emitter activity f is of particular interest, then smoothing a in a consistent way with filtering p may be rather important; see reconstructions given for phantom 2.

Finally, note that among different reconstruction algorithms in SPECT and PET there are, in particular, maximum likelihood algorithms (see [SV], [HL]) which take into account automatically the Poisson noise in the emission data and, therefore, do not require any prereconstruction filtration of these data. However, if an algorithm of reconstruction from data with Poisson noise in SPECT, PET or some other problem does not take yet automatically into account the noise statistic, then a prereconstruction data filtration may be necessary and then one can use, in particular, the filtration methods developed in the present work.

References

[BCB] Beis J S, Celler A and Barney J S 1995 An atomatic method to determine cutoff frequency based on image power spectrum *IEEE Trans. Nucl. Sci.* **42** 2250-2254

[BM] Bal G and Moireau P 2004 Fast numerical inversion of the attenuated Radon transform with full and partial measurements *Inverse Problems* **20** 1137-1164

[BS] Boman J and Strömberg J O 2004 Novikov's inversion formula for the attenuated Radon transform - A new approach *Journal of Geometric Analysis* **14** 185-198

[Br] Bronnikov A.V. 2000 Reconstruction of attenuation map using discrete consistency conditions *IEEE Trans. Med. Imaging* **19** 451-462

[C] Comtat C (2002) Méthodes de rétroprojection filtrée, *EPU SFPM-SFBMN, Traitement et analyse de données en médecine nucléaire*, Rouen, 13-15 mars 2002

[GB] Goodman J W and Belsher J F 1976 Fundamental limitations in linear invariant restoration of atmospherically degraded images *Imaging though Atmosphere SPIE* **75** 141-154

[GouNol] Gourion D and Noll D 2002 The inverse problem of emission tomography *Inverse Problems* **18** 1435-1460

[GJKNT] Guillement J-P, Jauberteau F, Kunyansky L, Novikov R and Trebossen R 2002 On single-photon emission computed tomography imaging based on an exact formula for the nonuniform attenuation correction *Inverse Problems* **18** L11-L19

[GN] Guillement J-P and Novikov R G 2004 A noise property analysis of single-photon emission computed tomography data *Inverse Problems* **20** 175-198

[HL] Hudson H M and Larkin R S 1994 Accelerated image reconstruction using ordered subsets of projection data *IEEE Trans. Med. Imaging* **13** 601-609

[Ku] Kunyansky L A 2001 A new SPECT reconstruction algorithm based on the Novikov's explicit inversion formula *Inverse Problems* **17** 293-306 (E-print, m$p_$arc/00-342)

[LM] Lewitt R M and Matej S 2003 Overview of methods for image reconstruction from projections in emission computed tomography *Proc. IEEE* **91** 1588-1611

[MNOY] Morosumi T, Nakajima M, Ogawa K and Yuta S 1984 Attenuation correction methods using the information of attenuation distribution for single photon emission CT *Med. Imaging Technol.* **2** 20-29

[MIMIKIH] Murase K, Itoh H, Mogami H, Ishine M, Kawamura M, Iio A and Hamamoto K 1987 A comparative study of attenuation correction algorithms in single photon emission computed tomography (SPECT) *Eur.J.Nucl.Med.* **13** 55-62

[Na] Natterer F 2001 Inversion of the attenuated Radon transform *Inverse Problems* **17** 113-119

[NW] Natterer F and Wübbelling F 2001 Mathematical Methods in Image Reconstruction (Philadelphia, PA: SIAM)

[No] Novikov R G 2002 An inversion formula for the attenuated x-ray transformation *Ark. Mat.* **40** 145-167

[RL] Rattey P A and Lindgren A G 1981 Sampling the 2-D Radon Transform *IEEE Trans. Acoust. Speech Signal (Proc. ASSP-29)* 994-1002

[SV] Shepp L A and Vardi Y 1982 Maximum likelihood reconstruction for emission tomography *IEEE Trans. Med. Imaging* **2** 113-122